

# Temperature and Gas Production Distributions on the Surface of a Spherical Model Comet Nucleus in the Orbit of 46P/Wirtanen

Achim Enzian

Jet Propulsion Laboratory, California Institute of Technology,  
Earth and Space Sciences Division, MS 183-601, Pasadena, CA, 91109  
Phone: (818) 393-5154 ; Email: Achim.Enzian@jpl.nasa.gov

Jürgen Klinger

Laboratoire de Glaciologie et de Géophysique de l'Environnement du  
CNRS, B.P. 96, F-38402 St Martin d'Hères

Gerhard Schwehm

ESA/ESTEC, Space Science Department, NL-2200 AG Noordwijk

Paul Weissman

Jet Propulsion Laboratory, California Institute of Technology,  
Earth and Space Sciences Division, MS 183-601, Pasadena, CA, 91109

submitted to Icarus on March 16, 1998  
revised on July 27, 1998

running title: Modeling of cometary nuclei.

# 1 Abstract

A multidimensional comet nucleus model is used to estimate the temperature and gas production distributions on the surface of a comet nucleus in the orbit of 46P/Wirtanen. The spherical model nucleus is assumed to be made up of a porous dust-ice ( $\text{H}_2\text{O}$ , CO) matrix. Heat and gas diffusion inside the rotating nucleus are taken into account in radial and meridional directions. A quasi-3D solution is obtained through the dependency of the boundary conditions on the local solar illumination as the nucleus rotates. As a study case, we consider a homogeneous chemical composition of the surface layer which is assumed to contain water ice. The model results include the distributions of temperature and gas production on the surface. For the chosen test case of a nucleus spin axis perpendicular to the orbital plane we found that the CO gas production on the surface is quasi uniformly distributed in contrast to the non-uniform water outgassing. The mixing ratio at a specific point on the comet nucleus surface is not representative of the overall mixing ratio which is observed in the coma.

**Keywords:** comets, comet nuclei, 46P/Wirtanen, modeling , Rosetta

## 2 Introduction

Periodic comet 46P/Wirtanen is the current target of the International Rosetta Mission, which will study the onset and evolution of cometary activity from a heliocentric distance of 4 astronomical units (AU) to perihelion at 1.08 AU. In order to plan for the encounter and to maximize the results of the mission, it is important to estimate the environment at the nucleus surface and in the near-nucleus coma.

The purpose of this paper is to present our quasi-3D comet nucleus model and to describe some initial model results such as the distributions of temperature and gas production on the surface of a spherical model comet nucleus in the orbit of comet 46P/Wirtanen. Special attention is paid to the possible outgassing of molecules more volatile than water. We choose CO as an example of an abundant volatile molecule in cometary nuclei, but other molecules such as CO<sub>2</sub>, CH<sub>4</sub> or N<sub>2</sub> could also be included in the model.

The comet nucleus model used in the present work was previously applied to simulations of comet 29P/Schwassmann-Wachmann 1 (Enzian 1997; Enzian *et al.* 1997) and comet Hale-Bopp (Enzian *et al.* 1998). In both works it was possible to predict the evolution of the carbon monoxide production rate which was confirmed by spectroscopic observations. The main advantages of our model compared to earlier published models are its higher spatial resolution of the nucleus surface as well as a 2-dimensional resolution of the diffusion equations.

Most of the comet nucleus models published so far have typically used the fast rotator approximation of a sphere (e.g., Espinasse *et al.* 1991, Tan-

credi *et al.* 1994, Podolak and Prialnik 1996) which averages the solar heat flux received by the projected comet nucleus disc over the total surface of a sphere. Diffusion equations for heat and gas are numerically integrated exclusively for the radial direction. In the fast rotator approximation the temperature and gas production distributions on the comet nucleus surface are assumed to be uniform and the diurnal variation of the solar flux cannot be resolved. Unlike this approximation, physico-chemical reactions such as sublimation are non-linear with respect to temperature. The advantage of the fast rotator approximation is that it is computationally simple and one can chose a larger integration time step for the boundary conditions. In the following we will call this class of models a 1-dimensional model. The fast rotator approximation can be improved by averaging the received solar flux only over the longitudes for individual latitudes instead of both the latitudes and the longitudes (e.g., Capria *et al.* 1996, Coradini *et al.* 1997).

A second class of models uses the so called slow rotator approximation in which the diurnal variation of the solar flux is taken into account. The energy balance of the comet nucleus surface in these models is written for a single rotating surface element (e.g., Benkhoff and Boice 1996) or for a large number of rotating surface elements (e.g., Weissman and Kieffer 1981, 1984). The slow rotator approximation allows one to compute the temperature and gas production distributions on the comet nucleus surface. To distinguish these models from the fast rotator models we define them as 1.5D models where the half dimension comes from the rotation or the hour angle. If in addition the model takes into account the lateral flux in the meridional

direction, like the Weissman and Kieffer model or this work, then we call it a 2.5D model, or quasi-3D model.

In this work we use the slow rotator approximation. The surface is described with a grid of 1000 geographical points which are distributed over the entire comet nucleus surface. The diffusion equations are integrated for the radial and meridional directions. A quasi-3D solution is obtained by relating the boundary conditions to the local solar illumination as the nucleus rotates. Although 2D and 3D diffusion effects are relatively small for a spherical nucleus (see also Benkhoff and Huebner, 1996) they can become important for more complex geometries which we want to study in the future. In addition to the features of the earlier multidimensional model of Weissman and Kieffer, our model takes into account chemical differentiation of ices more volatile than water.

### 3 Model description

In this section we describe the assumptions and hypotheses of the comet nucleus model used in the present study. The model solves a system of coupled reaction-diffusion equations which describes heat and gas diffusion in a porous material. Heat and mass exchange between the solid and the gas phase are taken into account. The solar heat flux, which is defined by the current orbit of comet Wirtanen, is absorbed by the surface layer. The model provides the temperature field within the nucleus, quantifies the redistribution of volatile molecules (through sublimation, gas diffusion and recondensation) and predicts the quantities of released gas and dust.

### 3.1 Composition

The model nucleus is assumed to be composed of porous ice-dust aggregates. The dust component represents a non-volatile phase which reduces the bond albedo of the water ice and dust. The ice constituent is composed of carbon monoxide enriched water ice which is initially in crystalline state. The condensed CO may evaporate by temperature controlled sublimation. The composition of the solid ice-dust matrix is described by the mass per unit volume of each constituent ( $\tilde{\rho}_i$  with  $i \equiv \text{dust, H}_2\text{O, or CO}$ ). The bulk density of the matrix,  $\rho$  can then be written as

$$\rho = \tilde{\rho}_d + \tilde{\rho}_{\text{H}_2\text{O}} + \tilde{\rho}_{\text{CO}} \quad (1)$$

The porosity,  $\Psi$ , which is here defined as the ratio of the pore volume to total volume of the matrix, is given by comparing the mass per unit volume of each constituent with the density of a compact solid ( $\rho_d, \rho_{\text{H}_2\text{O}}, \rho_{\text{CO}}$ ).

$$\Psi = 1 - \frac{\tilde{\rho}_d}{\rho_d} - \frac{\tilde{\rho}_{\text{H}_2\text{O}}}{\rho_{\text{H}_2\text{O}}} - \frac{\tilde{\rho}_{\text{CO}}}{\rho_{\text{CO}}} \quad (2)$$

### 3.2 Physico-chemical reactions

Below the nucleus surface the material is assumed initially to be in thermodynamic equilibrium. A small temperature rise induces sublimation. It can be shown that the characteristic time scale of sublimation is much shorter than those of heat and gas diffusion. Hence, the gas should be close to saturation if sufficient ice is present. Significant deviation from saturation can exist close to a sublimation front. From the saturation condition we can

define a source/sink term for the amount of gas sublimated from the ice per unit volume  $\dot{P}_i^{subl}$  ( $i \equiv \text{H}_2\text{O}$  or  $\text{CO}$ ).

$$\dot{P}_i^{subl} = \Psi \partial (p_i^{sat} - p_i) / \partial t \quad (3)$$

with the saturated vapor pressure  $p_i^{sat}$  and the partial gas pressure  $p_i$ . The sublimation leads to an enthalpy change  $\dot{H}_i^{subl}$  of

$$\dot{H}_i^{subl} = L_i^{subl} \frac{m_i}{k_B T} \dot{P}_i^{subl} \quad (4)$$

where  $L_i^{subl}$  is the latent heat of sublimation,  $m_i$  is the molecular mass and  $k_B$  is the Boltzmann constant. The gas and the solid phase are assumed to have the same temperature  $T$ .

### 3.3 Diffusion equations

The transport of heat and gas is defined by means of a system of three coupled diffusion equations ( $i \equiv \text{H}_2\text{O}$ ,  $\text{CO}$ ).

$$\rho c_p \frac{\partial T}{\partial t} = \nabla (K \nabla T) + \sum_i \dot{H}_i \quad (5)$$

$$\frac{\partial p_i}{\partial t} = \underbrace{\nabla (D_i^d \nabla p_i)}_{\text{diffusive}} + \underbrace{\nabla (D_i^v \nabla p)}_{\text{viscous}} + \sum_i \dot{P}_i \quad (6)$$

Where  $\rho$  is the density,  $c_p$  is the specific heat and  $K$  is the effective thermal conductivity of the solid phase. Additional heat sources for sublimation and advection are represented by source terms  $\dot{H}_i$ . The gas diffusion equations apply to viscous, free molecular (Knudsen) and mutual (Fick) diffusion.  $p_i$  is the partial pressure of species  $i$  and  $p = p_i + p_j$  is the total gas pressure of a binary gas mixture.  $D_i^d$  and  $D_i^v$  are the diffusion coefficients for diffusive

and viscous flow which are adopted from the Chapman-Enskog method. An additional gas source for sublimation and recondensation is denoted by  $\dot{P}_i$ .

The possible range of the thermal diffusivity of cometary materials is not well determined. We use a parameterized expression for the effective thermal conductivity. A structural change of the porous material such as through sintering is not taken into account. We intend to include sintering in a future version of this model.

$$K = h \left( \frac{\tilde{\rho}_{\text{H}_2\text{O}}}{\rho_{\text{H}_2\text{O}}} K_{\text{H}_2\text{O}} + \frac{\tilde{\rho}_{\text{CO}}}{\rho_{\text{CO}}} K_{\text{CO}} + \frac{\tilde{\rho}_d}{\rho_d} K_d \right) + 4r_p \epsilon \sigma T^3 \quad (7)$$

where  $K_i$  stands for the heat conductivity of the compact material of each solid phase. The parameter  $h$  is generally called the hertz factor and describes the efficiency of the grain-grain connection. Throughout one simulation we use a constant value for  $h$ . The last term of equation 7 accounts for the heat transport by means of thermal radiation, where  $r_p$  is a characteristic pore size,  $\epsilon$  is the infrared emissivity and  $\sigma$  is the Stefan-Boltzmann constant.

### 3.4 Boundary conditions

The diffusion equations are solved for two spatial dimensions ( $r$ , radius and  $\theta$ , co-latitude) using spherical coordinates. Each diffusion equation has two boundary conditions per dimension. The flux of the heat and gas diffusion at the nucleus center and at both geographic poles is set to zero.

$$\left. \frac{\partial T}{\partial r} \right|_{r=0} = 0, \quad \left. \frac{\partial T}{\partial \theta} \right|_{\theta=0} = 0, \quad \left. \frac{\partial T}{\partial \theta} \right|_{\theta=\pi} = 0$$

$$\left. \frac{\partial p_i}{\partial r} \right|_{r=0} = 0, \quad \left. \frac{\partial p_i}{\partial \theta} \right|_{\theta=0} = 0, \quad \left. \frac{\partial p_i}{\partial \theta} \right|_{\theta=\pi} = 0$$

At the surface, the temperature is inferred from the energy balance of a sublimating, conducting layer of finite thickness,  $dr$ :

$$\frac{S(1-A)}{r_h^2} \cos z = \epsilon \sigma T^4 + L_{\text{H}_2\text{O}}^{\text{subl}} \dot{Z}_{\text{H}_2\text{O}} + K \nabla T + dr \dot{H} \quad (8)$$

where  $S$  is the solar constant at 1 AU,  $r_h$  is the heliocentric distance and  $A$  is the bond albedo. The zenith angle of the Sun  $z$  is a function of the declination of the Sun as well as the latitude and the hour angle of each nucleus surface element.  $L_{\text{H}_2\text{O}}^{\text{subl}}$  is the latent heat of sublimation for water ice and  $\dot{Z}_{\text{H}_2\text{O}}$  is the mass loss rate per unit surface area and unit time

$$\dot{Z}_{\text{H}_2\text{O}} = \alpha p_{\text{H}_2\text{O}}^* \sqrt{\frac{m_{\text{H}_2\text{O}}}{2\pi k_B T}} \quad (9)$$

where  $\alpha$  is a correction for the effective fraction of the nucleus surface covered by ice

$$\alpha = \frac{\tilde{\rho}_{\text{H}_2\text{O}}}{\tilde{\rho}_{\text{H}_2\text{O}} + \frac{\rho_{\text{H}_2\text{O}}}{\rho_d} \tilde{\rho}_d} \quad (10)$$

$p_{\text{H}_2\text{O}}^*$  is the gas pressure of the evolving water at the surface, and  $m_{\text{H}_2\text{O}}$  is the mass of a water molecule. The thermal inertia of the surface layer is represented by the enthalpy change term  $dr \dot{H}$  which has the effect of decreasing the diurnal temperature variation.  $dr$  is the thickness of the surface layer in which the solar heat flux is absorbed. A good choice is to assume that  $dr$  equals the mean optical depth, which might be of the size of a grain (or a few grains for submicron-sized grains) in the case of a material having a low albedo. In the present work we choose the lower limit  $dr = 0$ .

The boundary conditions for the gas phase can in principle be determined by means of the mass balance at the surface. However, the gas flux from the

near-nucleus coma back to the nucleus surface can only be determined by using a hydrodynamical coma model. As the gas pressure above the nucleus surface is likely to be small as compared to the pressure below the surface, we set the gas pressure at the surface to zero. It was recently shown by Crifo and Rodionov (1998) that in case of a non-spherical nucleus the gas pressure in the near-nucleus coma can increase significantly in a topography with concave geometry. It would be interesting to couple such a coma model to our nucleus model to see how the surface temperature and gas production rates are affected.

During each time step the local gas production rates are determined for a fraction of the nucleus surface ( $S = 4\pi R_N^2/N$ , where  $N$  is the nucleus spin period divided by the time step) represented by a wedge of surface elements aligned along a meridian. This surface wedge is rotated with the nucleus spin period. After one rotation the global gas production rates are calculated by summing the local outgassing rate for each surface element.

$$\dot{Q}_{\text{H}_2\text{O}} = \sum_{t=t_0}^{t=t_0+Ndt} S \sum_{\text{meridian}} \left( D_{\text{H}_2\text{O}}^d \nabla p_{\text{H}_2\text{O}} + D_{\text{H}_2\text{O}}^v \nabla p + \Delta Z_{\text{H}_2\text{O}} \right) \quad (11)$$

$$\dot{Q}_{\text{CO}} = \sum_{t=t_0}^{t=t_0+Ndt} S \sum_{\text{meridian}} \left( D_{\text{CO}}^d \nabla p_{\text{CO}} + D_{\text{CO}}^v \nabla p \right) \quad (12)$$

Surface erosion due to sublimation is computed as a function of latitude. However, for reasons related to the computational efficiency the model considers that the overall shape of the nucleus remains spherical. We are currently working on a new model version where we will take into account the evolution of the nucleus shape.

The model considers the test case of a constant dust to ice mass ratio

at the nucleus surface. This assumption is realistic only for a low cohesion force between dust grains. In a future version of our model we plan to take into account a gas dynamical description of the grain ejection process (e.g., Coradini *et al.* 1997). However, as the cohesion force between grains is not determined yet we prefer to test extreme cases of a very low cohesion (corresponding to free surface sublimation) and a very high cohesion force (accumulation of dust grains at the surface) instead of choosing some arbitrary intermediate case.

Further details of the numerical code can be found in Enzian *et al.* (1997).

## 4 Physical and numerical parameters

The most important physical parameters used for this work are shown in Table 1. The parameters used are chosen from the parameter list as defined by the Comet Nucleus Working Team (Huebner *et al.* 1998).

In the model we assume a spherical shape for the comet nucleus composed of a porous dust-ice ( $\text{H}_2\text{O}$ , CO) mix. At the beginning of the simulation the nucleus has a homogeneous composition and a uniform temperature of 20 K. At such a low temperature CO remains in the solid phase. The CO is considered as an independent phase (5% of the total nucleus mass). The initial nucleus composition has a dust-to-ice mass ratio of 1, which corresponds to the lower value estimated for comet 1P/Halley (McDonnell *et al.* 1991). The compact dust density is assumed to be  $3250 \text{ kg m}^{-3}$ . A density of  $917 \text{ kg m}^{-3}$  is chosen for both of the volatile ice phases. The initial bulk mass density is  $500 \text{ kg m}^{-3}$  which is a mean value of Rickman's density estimation for comet

1P/Halley (Rickman, 1986). We should mention that Sagdeev *et al.* 1988 and Peale (1989) suggested bulk densities in the range of  $200 < \rho < 1500 \text{ kg m}^{-3}$ . Recently, Rickman revised his estimates leading to a higher density but still below  $1000 \text{ kg m}^{-3}$  (Rickman, 1998). The density of  $500 \text{ kg m}^{-3}$  in our model leads to an initial porosity of 0.65. The initial pore radius is chosen to be  $10^{-4} \text{ m}$ . During the simulation the pore radius increases with porosity.

The thermal conductivity of compact crystalline water ice is given by Klinger (1980)

$$K_{\text{H}_2\text{O}}^c = \frac{567}{T} \text{ W m}^{-1} \text{ K}^{-1} \quad (13)$$

The specific heat of water ice has been fitted by Klinger (1980) from measured data given by Giaque and Stout (1936).

$$c_{p,\text{H}_2\text{O}} = 7.49 T + 90 \text{ J kg}^{-1} \text{ K}^{-1} \quad (14)$$

For CO we use the upper limit suggested by Tancredi *et al.* (1994):  $c_{p,\text{CO}} = 2010 \text{ J kg}^{-1} \text{ K}^{-1}$ .

The saturated vapor pressures of the volatile molecules are approximated by

$$p_i^{\text{sat}} = A_i \exp(-E_i/T) \quad (15)$$

where  $A_{\text{H}_2\text{O}} = 3.56 \times 10^{12} \text{ N m}^{-2}$ ,  $E_{\text{H}_2\text{O}} = 6141.667 \text{ K}$  (Fanale and Salvail 1984) and  $A_{\text{CO}} = 1.6624 \times 10^9 \text{ N m}^{-2}$ ,  $E_{\text{CO}} = 764.16 \text{ K}$  (Fanale and Salvail 1990). More precise formulae for the vapor pressure exist (e.g., Washburn 1928, Kouchi 1987). However, taking into account the uncertainty in the description of the sublimation process we have chosen equation 15 as it allows more efficient computation. The latent heat of sublimation is assumed to be

equal to the activation energy  $E_i$  in order to be consistent with the equation for the saturated vapor pressure (equation 15).

The spherical cometary nucleus with radius  $R_N$  is subdivided into 100 concentric shells. The thickness of the first 20 shells is 0.05 m. Beyond the depth of 1 meter the thickness of the shells increases by an exponentially growing step size. Each meridian is divided into 20 latitudinal elements. The parallels are divided into 50 elements of equal size so that the numerical time integration step,  $dt$ , becomes 0.02 of the nucleus spin period. The distribution of surface elements on the modeled nucleus is shown in figure 1.

## 5 Results and discussion

We present results for a model of comet 46P/Wirtanen assuming a spherical nucleus with a spin axis perpendicular to the orbital plane. We ran the model over five orbits of the comet, starting at aphelion. The instantaneous surface temperature distribution at 1.08 AU (perihelion) and at 3 AU (where most of the experiments onboard the ROSETTA spacecraft will start) from the Sun on the fifth orbit is shown in figure 2. In the case of a freely sublimating ice-dust surface (see the two plots in figure 2 at left) the maximum surface temperature is 205 K for an albedo of 0.04, significantly below the black body temperature at this solar distance of 377 K. The computed maximum surface temperature is a lower limit as dust is not allowed to accumulate on the surface. The temperature distribution in longitude is asymmetric with respect to the subsolar point as expected due the thermal inertia of the surface.

Unlike the freely sublimating surface, the temperature of a dust covered nucleus surface (layer of 10 cm in thickness is depleted of ice at the equator) is significantly higher (see the two plots in figure 2 at right) and approaches the black body radiation equilibrium. This is due to the assumed low heat conduction of the porous dust layer:  $0.1 \text{ W m}^{-1} \text{ K}^{-1}$ . However, in this case the remaining heat available for sublimation is significantly lower than in the first case. As a consequence, the outgassing rate for water is several orders of magnitude lower than in the case of a freely sublimating surface and doesn't compare favorably with observations of comet P/Wirtanen (figure 7). The results for the dust covered case are not discussed further in this paper.

The surface temperature of real comets is currently inaccessible by remote sensing due to the thermal emission of the coma and due to the lack of spatial resolution on the nucleus surface using Earth-based instruments. However, during the last perihelion passage of comet Halley in 1986, the IKS thermal imager onboard the Vega 1 spacecraft detected an IR emission source a few kilometers in size in the nucleus direction, with a temperature of  $420 \pm 60 \text{ K}$  (Combes *et al.* 1986; Emerich *et al.* 1991). Such a temperature, far beyond the triple point of water, suggests that at least a fraction of the Halley nucleus surface was covered by a refractory layer. An alternative explanation is that the IR emission corresponded to a dust filament in the inner coma of Halley which coincided with the line of sight. Based on this data Combes and co-workers could neither confirm nor exclude the presence of water ice, as its thermal emission would be hidden by the high temperature emission source.

The evolution of the modeled surface temperature versus heliocentric dis-

tance is shown in figure 3. For the same heliocentric distance, the surface temperatures after perihelion are higher than before perihelion, for each latitudes. The higher latitudes receive less solar flux and the thermal conduction term in the surface energy balance becomes relatively more important compared to the energy dissipation through sublimation and thermal radiation. The non-linear behavior of the dissipation terms causes the thermal inertia to be more significant at higher latitudes.

An example of the temperature profile versus depth is shown in figure 4. The plots show profiles for three different latitudes at 1.08 AU and 3 AU from the Sun, after five orbits. The diurnal thermal skin depth is about 20 cm.

The instantaneous water production distribution on the nucleus surface at perihelion and at 3 AU from the Sun for the nucleus without a dust mantle is shown in figure 5. Water outgassing is produced mainly through free sublimation at the nucleus surface. Thus, the production rates are strongly correlated with the surface temperature distribution. Gas production from sublimating icy grains in the coma is not taken into account.

Unlike the water production distribution, the carbon monoxide outgassing is near-uniform along lines of constant latitude because the CO source is situated below the surface, deeper than the diurnal thermal skin depth. The CO sublimation front penetrates into the inner part of the nucleus. Although the nucleus surface is receding due to the loss of water ice and entrained dust, the erosion can't catch up with the greater penetration of the CO sublimation front (figure 6). The depth of the CO sublimation front depends on the amount of CO in the initial mix. The depth predicted by our model is some

tens of meters.

Both the inhomogeneous water production and the non-uniform surface temperature distribution suggest an asymmetric coma expansion. Even in the case of nearly isotropic outgassing, as predicted for CO, the gas density at the nucleus surface is asymmetric due to the non-uniform surface temperature distribution. In addition, local inhomogeneities in chemical composition or an irregular nucleus shape will amplify the development of structures in the inner coma. The formation of such coma structures was shown by gas dynamical modeling of a dusty coma (Crifo and Rodionov 1997). Using CO production rates obtained from the model results presented in the current work, Crifo and Rodionov showed that in the near-nucleus coma the gas phase is capable of efficiently accelerating dust, even at 3 AU from the Sun.

## 6 Comparison with observations

### 6.1 Water production rates

The presence of water vapor in the Earth's atmosphere does not permit detection of cometary H<sub>2</sub>O from ground-based observations. Typically, water production rates are estimated from production rates of the OH radical and atomic hydrogen, which are assumed to be produced by photodissociation of H<sub>2</sub>O molecules. During the perihelion passage of comet Wirtanen in 1996, Farnham and Schleicher (1997) derived an OH production rate of  $7.8 \times 10^{27}$  molecules/s at 1.07 AU from the Sun, using narrow-band photometry. A similar water production rate,  $7 \times 10^{27}$  molecules/s, was reported by Bertaux (1997) from an analysis of the Lyman-alpha emission of the hydrogen enve-

loped, which could be observed by the SWAN experiment onboard the SOHO spacecraft. Different radii for the model comet nucleus have been tested. For a comet nucleus radius of about 600 m, the radius suggested by observations, the observed production rates at perihelion compare more favorably with our predicted value of  $10^{28}$  molecules/s for P/Wirtanen. Our result confirms that comet Wirtanen has a small nucleus compared to most measured comets. Böhnhardt *et al.* (1996) suggested an upper limit on the nucleus radius of 0.8 km from a detection at 4.6 AU. More recently, Lamy (1996) used the WFPC2 camera on the HST to image the inner coma of P/Wirtanen in an attempt to detect the nucleus. Taking into account a coma correction, Lamy estimated a mean effective radius of 0.58 km (both estimates assume a geometric albedo of 0.04). Our thermo-physical estimate of about 600 m is compatible with HST observations.

Another method of estimating water production consists of converting the comet's light curve to  $\text{H}_2\text{O}$  production rates,  $\dot{Q}_{\text{H}_2\text{O}}$ , by using an empirical relation given by Jorda (1995) between  $\dot{Q}_{\text{H}_2\text{O}}$  and the heliocentric magnitude  $m_h$

$$\log \dot{Q}_{\text{H}_2\text{O}} = 30.78(\pm 0.25) - 0.265 \times m_h. \quad (16)$$

This relation was obtained from a data analysis of 15 comets closer than 2.8 AU to the Sun and having a water production rates larger than  $10^{28}$  molecules/s.

A comparison between water production rates derived from the visual brightness of comet P/Wirtanen and modeled rates for a comet nucleus with a radius of 600 m is shown in figure 7. Taking into account the uncertainty in the nucleus size (due to the unknown albedo and coma corrections), one

can note the general agreement between the modeling and the observations at perihelion. The slope of the water production rates beyond 1.5 AU (pre-perihelion in 1996), however, cannot be explained by our model. A better agreement might be obtained if the model assumed a partially dust covered nucleus surface beyond 3 AU from the Sun, but with the dust cover removed as the solar flux increases. Other explanations such as a change in the size distribution of the dust grains are also possible. On the other hand, it is not clear if the correlation formula used is valid for faint objects like comet P/Wirtanen, having production rates lower than  $10^{28}$  molecules  $s^{-1}$ .

## 6.2 CO production rates

Distant activity of cometary nuclei has been observed since at least the discovery of comet 29P/Schwassmann-Wachmann 1 (P/S-W 1). Radio spectroscopic observations of P/S-W 1 showed that outgassing of carbon monoxide appears to be the driver of the observed distant activity (Senay and Jewitt 1994; Crovisier *et al.* 1995). More recently, observations of comet Hale-Bopp have led to a similar conclusion (Biver *et al.* 1997). Both P/S-W 1 and Hale-Bopp have a nucleus size of a few tens of kilometers, which is significantly larger than the typical size of observed short-period Jupiter family comets. It is not clear if distant cometary activity is a selection artifact for large bodies or if such bodies have significantly different chemical compositions. If all comets have a similar origin, there should be no substantial difference in their initial composition. However, it is expected that during the temporal evolution of a comet in the inner solar system the near-surface initial com-

position is lost by chemical differentiation as more volatile ices sublime or are freed by the amorphous-crystalline water ice transition.

Comet Wirtanen has a small nucleus and even if CO was produced by the same mechanism as in comets Hale-Bopp or P/S-W 1, it could not have been detected due to the instrumental detection limit of the order of  $4 \times 10^{27}$  molecules/s (D. Bockelée-Morvan, personal communication). A significant improvement on the current detection limit is predicted for the MIRO experiment onboard the Rosetta spacecraft, to be launched in 2003. The evolution of the CO production rates calculated by the model is shown in figure 8. In the model carbon monoxide sublimates from a subsurface layer. The depth of the sublimation front increases with the temporal evolution and the production rate decreases (figure 6). In contrast to the water production rate, the CO production rate after perihelion passage is larger than before perihelion. This behavior is explained by the thermal inertia of the layers between the surface and the sublimation front of the CO. The predicted outgassing rate for CO is almost identical for the freely sublimating icy surface and the dust covered surface. For this reason only the freely sublimating case is shown in figure 8.

As no direct observations of CO exist for P/Wirtanen, we used an empirical formula given by Di Folco and Bockelée-Morvan (1997) which has been derived for comet Hale-Bopp from the correlation between the measured CO production rate and the brightness

$$\log \dot{Q}_{\text{CO}} = 30(\pm 0.04) - 0.256(\pm 0.009) \times m_{r_h} \quad (17)$$

This expression is valid only for heliocentric distances larger than 3 AU

where CO was observed to be the most abundant molecule in the coma of comet Hale-Bopp. CO production rates derived from observed magnitudes of P/Wirtanen at  $r_h > 3$  AU are shown in figure 8. However, the dashed line in figure 8 shows the apparent production rates corresponding to the expected magnitude of a 600 m cometary nucleus with an albedo of 0.04 . From the comparison with the available observational data from observation, we cannot conclude that there was any CO production from P/Wirtanen in 1996.

It is believed that comet nuclei such as P/Wirtanen are strongly differentiated bodies as a result of their thermal evolution in a short-period comet orbit. Therefore we have to be careful in the interpretation of the model results, in particular with respect to the CO outgassing rates. The assumption of an initially homogenous composition is likely not justified. In addition, the limited integration time over a few tens or hundreds of years, assuming the current orbits or even a trajectory from the Kuiper belt might be too small compared to the age of the comet. We know that P/Wirtanen has made at least 9 orbits of the Sun since its discovery in 1947, and likely many more given the typical dynamical life time of Jupiter-family comets. Therefore we think that the computed CO production rates should be considered as upper limits. The lower limit would be zero CO production.

We want also to stress that the mixing ratios in the coma (e.g., CO/H<sub>2</sub>O) which are typically measured by observers do not represent the chemical composition of the bulk comet nucleus or of the comet nucleus surface. Also the mixing ratio at a specific point on the comet nucleus surface is not represen-

tative of the overall mixing ratio which is observed in the coma. As can be seen in figure 5 the mixing ratio is a function of both latitude and longitude.

## 7 Comparison with related work

Several groups of researchers have calculated the thermal evolution of a comet in the orbit of P/Wirtanen using thermo-physical comet models. All existing models used for this comparison consider a nucleus spin axis perpendicular to the orbital plane and all models assume a nucleus composed of dust, water ice, and one or more other more volatile molecules such as carbon monoxide. The main differences versus our model concern the description of the comet nucleus surface and the surface energy balance as well as the 2-dimensional resolution of the diffusion equations.

All models used for this comparison are 1-dimensional (Podolak and Prialnik 1996, Capria *et al.* 1996) or 1.5-dimensional models (Benkhoff and Boice 1996). We did not find in the literature multidimensional comet nucleus models which includes gases more volatiles than water.

The distributions of temperature and gas production on the comet nucleus surface are not computed by the works as noted above and therefore cannot be discussed with respect to our work. Among the results which we can compare, it is found by all models that after the formation of a dust mantle, the water production rate at perihelion drops by more than two orders of magnitude. This effect is due to the reduced energy available for water sublimation since the nucleus surface temperature is higher and thus more energy is lost through thermal radiation. The CO production rates are less

affected by the presence of a dust covered comet nucleus surface. Another interesting result is that the CO outgassing rates do not reach their maximum and minimum in phase with the heliocentric distance and the water production rates.

**Podolak and Prialnik (1996):** This model uses the fast rotator approximation of a sphere leading to an underestimation of the  $\text{H}_2\text{O}$  production rate with increasing heliocentric distance. Compared to our work, their model uses similar parameters for the initial density and heat conductivity. However, the values for the thermal emissivity and the albedo are 0.5 and 0.03, respectively. These values compare with our parameters of 0.96 and 0.04. In the Podolak and Prialnik model twice as much energy is available for sublimation of volatiles because of the low emissivity. The model takes into account crystallization of amorphous ice. Two different gases (4.5% CO and 0.5%  $\text{CO}_2$ , by mass) are initially trapped in the amorphous ice. The trapped gases are assumed to be released from the ice upon crystallization, without affecting the associated heat release. The gas may eventually condense in colder layers and sublimate from these layer once the layers are sufficiently heated. The predicted CO outgassing rates are almost constant throughout one orbit reaching a maximum production rate of  $10^{25}$  molecules/s after 10 orbits. The value of the water production rate at perihelion is  $5 \times 10^{27}$  molecules/s. This compares with our estimates of the production rates of  $9 \times 10^{25}$  molecules/s (CO) and  $10^{28}$  molecules/s ( $\text{H}_2\text{O}$ ), after five orbits. The production rates were scaled to a 600 m nucleus.

The fast rotator approximation assumes an isothermal surface tempera-

ture and a uniform distribution of the outgassing at the surface. Therefore it is not possible to compare results further with the distributions computed with our model.

**Benkhoff and Boice (1996):** This model uses the slow rotator approximation of a single rotating surface element. The model uses similar parameters for density, heat conductivity, emissivity and albedo. The chemical composition includes crystalline water ice (61-80% by mass), CO<sub>2</sub> (7-9%), CO (3.5-5.5%), CH<sub>4</sub> (3.5-5.5%) and dust (0-25%). The maximum surface temperature at the subsolar point at perihelion is 370 K for the dust covered comet nucleus surface and 200 K for the freely sublimating icy surface. This compares with our temperatures at the subsolar point of 358 K and 205 K, respectively. As only the maximum values of the gas production rates for the subsolar point are presented, it is difficult to compare them with the estimated production rates of our model. The maximum values for the water and CO production rates are  $10^{22}$  molecules m<sup>-2</sup> s<sup>-1</sup> and  $4 \times 10^{18}$  molecules m<sup>-2</sup> s<sup>-1</sup> (after five orbits), respectively. This compares with our estimates of the production rates at the subsolar point of  $10^{22}$  molecules m<sup>-2</sup> s<sup>-1</sup> and  $2 \times 10^{19}$  molecules m<sup>-2</sup> s<sup>-1</sup> for water and CO, respectively. The distribution of surface temperatures and outgassing rates are not computed.

**M. T. Capria *et al.* (1996):** The model of Capria and co-workers uses a fast rotator approximation, although different from the one used in the Podolak and Prialnik model. In this model, the solar flux received at a specific latitude is averaged over the hour angle. The diurnal variation of

the solar flux is not taken into account. The authors consider accumulation and emission of non-cohesive dust grains on the comet nucleus surface. The thermal behavior is simulated for a comet nucleus that starts from an orbit in the Kuiper belt, is injected into the giant planets region, and through multiple close encounters evolves into the present orbit of comet Wirtanen. The influence of the latitude on the evolution of the nucleus is analyzed with two models having two different latitudes:  $0^\circ$  and  $80^\circ$ . The model uses similar input parameter for density, heat conductivity, emissivity and albedo. The initial chemical composition includes amorphous water ice (47% by mass), CO (2.5%), CO<sub>2</sub> (0.5%) and dust (50%). The more volatile ices are trapped in the amorphous water ice and are released upon crystallization, taking into account the latent heat of evaporation. The Capria model predicts a maximum surface temperature at perihelion of about 200 K at the equator and 180 K at  $80^\circ$  latitude. The maximum temperatures at aphelion reach 130 K and 85 K for the equator and for  $80^\circ$  latitude, respectively. These temperatures compare favorably to ours in the case of a freely sublimating icy surface. The gas production rate is given only for the subsolar point and reaches a rate of about  $10^{18}$  molecules  $\text{m}^{-2} \text{s}^{-1}$  at perihelion. The water production includes very strong bursts of up to two orders of magnitude reaching  $10^{20}$  molecules  $\text{m}^{-2} \text{s}^{-1}$ . This peak value is about two orders of magnitude lower than the production rate predicted by the Benkhoff and Boice model as well as in our work. The likely explanation of this discrepancy is the presence of a dust mantle at the comet nucleus surface. The surges in water production could then be the result of a partial dust mantle blow-off.

However, in that case the surface temperature would have been expected to be significantly higher, unless one considers a dramatic increase in the heat conductivity of the dust mantle. The CO production is almost constant through one orbit and has a rate of  $10^{18}$  molecules  $\text{m}^{-2} \text{s}^{-1}$ . This compares favorably to our rates predicted for the subsolar point and to those of the Benkhoff and Boice model.

## 8 Conclusions

In this paper we have presented results of a multidimensional model of comet 46P/Wirtanen, assuming a spherical model nucleus with a spin axis perpendicular to the orbit plane. We found that 2D and 3D effects of the heat and gas diffusion are relatively small for a nucleus with a spherical shape. However, we think that these effects can become important for a more realistic, irregular nucleus shape. The main results of the model are the distributions of temperature and gas production on the nucleus surface. It was shown that the gas production rates and the outgassing mixing ratios above the comet nucleus surface depend strongly on latitude, longitude and heliocentric distance. Thus we conclude that it is very important to describe the comet nucleus surface with a large number of grid points. The modeled gas production rates are quantitatively compared against actual observations of P/Wirtanen. The important results are:

- The distribution of carbon monoxide outgassing on the nucleus surface is found to be near-uniform. The distributions of surface temperature

and water production, however, depend on the solar flux received at a given point on the nucleus surface.

- A water production rate of  $10^{28}$  molecules/s, close to that observed for comet Wirtanen at perihelion in 1996, can be explained by free surface sublimation of water ice from a comet nucleus composed of ice and dust and having a mean effective radius of about 600 m, the radius suggested by CCD observations.
- The calculated likely upper limits for carbon monoxide outgassing for a nucleus with a radius of 600 m is  $\sim 10^{26}$  molecules/s (after five orbits). This rate depends on the thermal history and the possible chemical differentiation inside the nucleus of comet Wirtanen.
- The model was compared with other comet nucleus models. The comparison is difficult as these models use a different description of the comet nucleus surface and do not provide the distributions of temperature and gas production on the surface.

## 9 Acknowledgements

A. Enzian is a Research Associate of the National Research Council (NRC / NASA). We thank Dr. J-F. Crifo (Service d'Aéronomie du CNRS) for comments on this work. Thanks also to Drs. D. Bockelée-Morvan (Observatoire de Paris- Meudon) and O. Hainaut (Institute for Astronomy, Honolulu) for providing observational data. The main part of this work was performed at Laboratoire de Glaciologie et Géophysique de l'Environnement in Grenoble

(F) and during a research visit at ESA's European Science and Technology Center in Noordwijk (NL). The paper was finished at the Jet Propulsion Laboratory, California Institute of Technology, under contract with NASA.

## References

- [1] J. Benkhoff and D. C. Boice. Modeling the thermal properties and the gas flux from a porous, ice-dust body in the orbit of P/Wirtanen. *Planet. Space Sci.*, 44:665–674, 1996.
- [2] J. Benkhoff and W. F. Huebner. Modeling of gas flux from a Jupiter-family comet nucleus. *Planet. Space Sci.*, 44:1005–1013, 1996.
- [3] N. Biver, D. Bockelée-Morvan, P. Colom, J. Crovisier, J. K. Davies, W. R. F. Dent, D. Despois, E. Gérard, E. Lellouch, H. Rauer, R. Moreno, and G. Paubert. Evolution of the outgassing of comet Hale-Bopp (C/1995 O1) from radio observations. *Science*, 275:1915–1918, 1997.
- [4] H. Bönnhardt, R. M. West, and J. Babion. Comet 46P/Wirtanen. *IAU Circ. No 6392*, 1996.
- [5] M. T. Capria, F. Capaccioni, A. Coradini, C. De Sanctis, S. E. C. Federico, R. Orosei, and M. Salomone. A P/Wirtanen evolution model. *Planet. Space Sci.*, 44:987–1000, 1996.
- [6] A. Coradini, F. Capaccioni, M. T. Capria, C. De Sanctis, S. Espinasse, R. Orosei, and M. Salomone. Transition elements between comets and asteroids. *Icarus*, 129, 317–336, 1997.

- [7] M. Combes, V. I. Moroz, J. F. Crifo, J. M. Lamarre, J. Charra, N. F. Sanko, A. Soufflotand, J. P. Bibring, S. Cazes, N. Coron, J. Crovisier, C. Emerich, T. Encrenaz, R. Gispert, A. V. Grigoryev, G. Guyot, V. A. Krasnopolsky, Y. V. Nikolsky, and F. Rocard. Infrared sounding of comet P/Halley from Vega 1. *Nature*, 321:266–268, 1986.
- [8] J. F. Crifo and A. V. Rodionov. The dependence of the circumnuclear coma structure on the characteristics of the nucleus. II First investigation of the coma surrounding an homogeneous, aspherical nucleus. *Icarus*, 129:72–93, 1997.
- [9] J. F. Crifo and A. V. Rodionov. Modelling of the circumnuclear coma of comets: objectives, methodes and recent results, *Planet. Space Sci.*, in press, 1998.
- [10] J. Crovisier, N. Biver, D. Bockelée-Morvan, P. Colom, L. Jorda, and E. Lellouch. Carbon monoxide outgassing from comet P/Schwassmann-Wachmann 1. *Icarus*, 115:213–216, 1995.
- [11] C. Emerich, J. M. Lamarre, V. I. Morez, M. Combes, N. F. Sanko, Y. V. Nikolksy, F. Rocard, R. Gispert, N. Coron, J. P. Bibring, T. Encrenaz, and J. Crovisier. Temperature and size of the nucleus of comet P/Halley deduced from IKS infrared Vega 1 measurements. *Astron. Astrophys.*, 187:839–842, 1991.

- [12] A.ENZIAN. *Modélisation multidimensionnelle du comportement thermodynamique des noyaux de comètes*. Doctoral thesis, Université Joseph Fourier, Grenoble I, 1997.
- [13] A.ENZIAN, H. CABOT, and J. KLINGER. A 2 1/2 D thermodynamic model of cometary nuclei: I Application to the activity of comet 29P/Schwassmann-Wachmann 1. *Astron. Astrophys.*, 319:995–1006, 1997.
- [14] S. ESPINASSE, J. KLINGER, C. RITZ, and B. SCHMITT. Modeling of the thermal behavior and of the chemical differentiation of cometary nuclei. *Icarus*, 92:350–365, 1991.
- [15] F. P. FANALE and J. R. SALVAIL. An idealized short period comet model: Surface insolation, H<sub>2</sub>O flux, dust flux, and mantle evolution. *Icarus*, 60:476–511, 1984.
- [16] F. P. FANALE and J. R. SALVAIL. The influence of CO ice on the activity and near-surface differentiation of comet nuclei. *Icarus*, 84:403–410, 1990.
- [17] E. D. FOLCO and D. BOCKELÉE-MORVAN. Master's thesis, Observatoire de Paris Meudon, Université Paris VII, 1997.
- [18] J. A. GHORMLY. Enthalpy changes and heat-capacity changes in the transformations from high-surface-area amorphous ice to stable hexagonal ice. *J. Chem. Phys.*, 48:503–508, 1968.

- [19] W. F. Giauque and J. W. Stout. The entropy of water and third law of thermodynamics. The heat capacity of ice from 15 K to 273 K. *J. Am. Chem. Soc.*, 58:1144–1150, 1936.
- [20] W. F. Huebner, J. Benkhoff, M. T. Capria, A. Coradini, C. De Sanctis, and A. Enzian) A reference comet nucleus model, In preparation, 1998.
- [21] L. Jorda. *Atmospheres cométaires: interprétation des observations dans le visible et comparaison avec les observations radio*. Doctoral thesis, Observatoire de Paris-Meudon, Université de Paris VII, 1995.
- [22] J. Klinger. Influence of a phase transition of ice on the heat and mass balance of comets. *Science*, 209:271–272, 1980.
- [23] A. Kouchi. Vapour pressure of amorphous H<sub>2</sub>O ice and its astrophysical implications. *Nature*, 330:550–552, 1987.
- [24] P. L. Lamy. Comet 46P/Wirtanen. *IAU Circ. No 6478*, 1996.
- [25] J. A. M. McDonnell, P. L. Lamy, and G. S. Pankiewicz. Physical properties of cometary dust. In R. L. Newburn Jr., M. Neugebauer, and J. Rahe, editors, *Comets in the Post-Halley Era*, volume 2, pages 1043–1074, Dordrecht, 1991. Kluwer Academic Publishers.
- [26] S. J. Peale. On the density of Halley’s comet. *Icarus*, 82:36–49, 1989.
- [27] M. Podolak and D. Prialnik. Models of the structure and evolution of comet P/Wirtanen. *Planet. Space Sci.*, 44:655–664, 1996.

- [28] H. Rickman. Masses and densities of comets Halley and Kopff. In C. Melita, editor, *Comet Nucleus Sample Return Mission*, pages 195–205, Noordwijk, The Netherlands, 1986. ESA SP-249.
- [29] H. Rickman. On the density of cometary nuclei. *Abstracts of the IAU Colloquium 168 in Nanjing*, 1998.
- [30] R. Z. Sagdeev, P. E. Elyasberg, and V. I. Moroz. Is the nucleus of comet Halley a low density body ? *Nature*, pages 240–242, 1988.
- [31] M. C. Senay and D. Jewitt. Coma formation driven by carbon monoxide release from comet Schwassmann-Wachmann 1. *Nature*, 371:229–231, 1994.
- [32] G. Tancredi, H. Rickman, and J. M. Greenberg. Thermochemistry of cometary nuclei. *Astron. Astrophys.*, 286:659–682, 1994.
- [33] E. Washburn. *International Critical Tables*, volume 3. 1928.
- [34] P. R. Weissman and H. H. Kieffer. Thermal modeling of cometary nuclei. *Icarus*, 47:302–311, 1981.
- [35] P. R. Weissman and H. H. Kieffer. An improved thermal model for cometary nuclei. *Journal of Geophysical Research*, 89:C358–C364, 1984.

Semimajor axis		3.115 AU
Orbit eccentricity		0.655
Spin period		24 hours
Spin axis		perpendicular to orbital plane
Nucleus radius	$R_N$	600 m
Bond albedo	$A$	0.04
Infrared emissivity	$\epsilon$	0.96
Initial nucleus temperature		20 K
Hertz factor	$h$	0.01
Nucleus bulk density	$\rho$	500 kg m <sup>3</sup>
Bulk thermal conductivity of dust	$K_d$	10 W m <sup>-1</sup> K <sup>-1</sup>
Pore radius	$r_p$	10 <sup>-4</sup> m
Chemical composition		
H <sub>2</sub> O		0.45 (mass ratio)
CO		0.05
Dust		0.50

Table 1: Physical input parameters where chosen from the parameter set defined by the Comet Nucleus Working Team (Huebner *et al.* 1998).

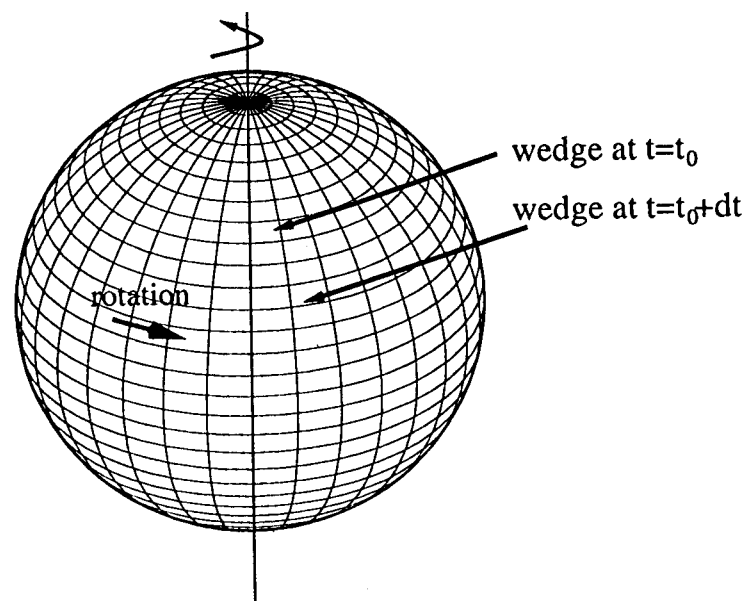


Figure 1: Schematic view of the modeled comet nucleus.

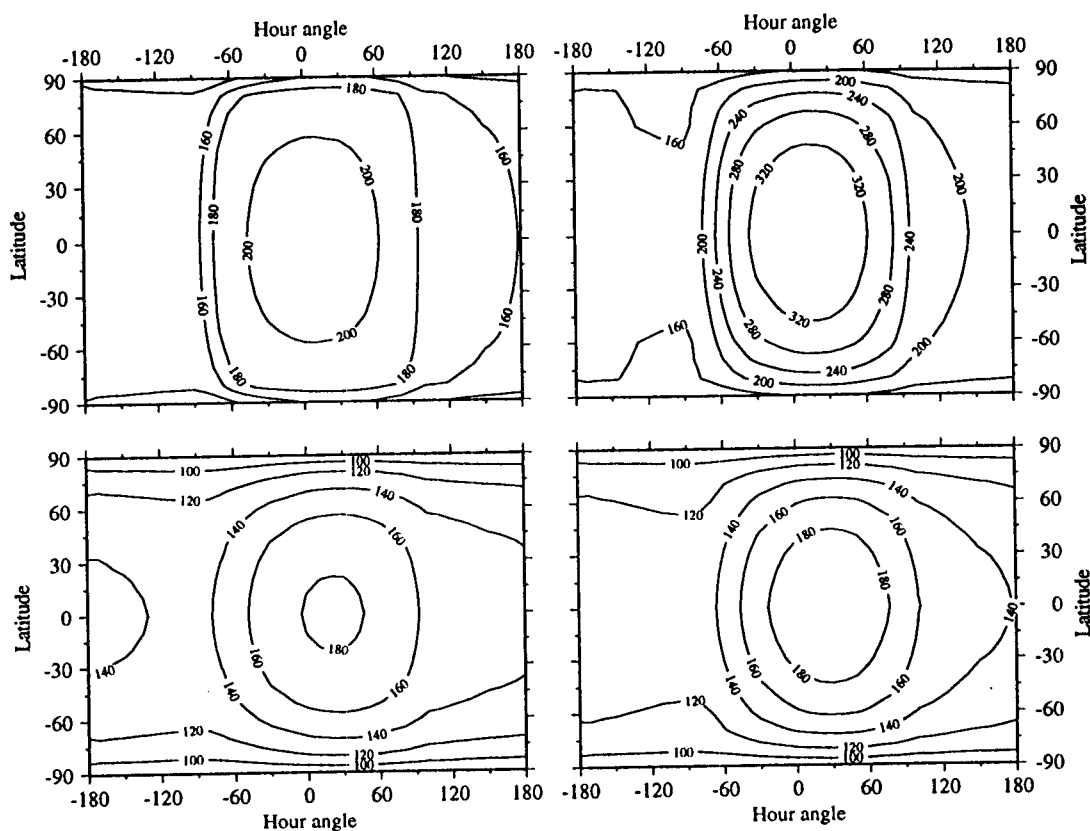


Figure 2: Temperature distribution at the surface of the modeled comet nucleus (in Kelvin) at 1.08 AU (top) and 3 AU (bottom) from the Sun, after five orbits. The temperatures for a freely sublimating ice-dust surface are shown in the two figures at left. The temperatures for a dust covered cometary nucleus are shown at right. The nucleus spin axis is perpendicular to the orbital plane.

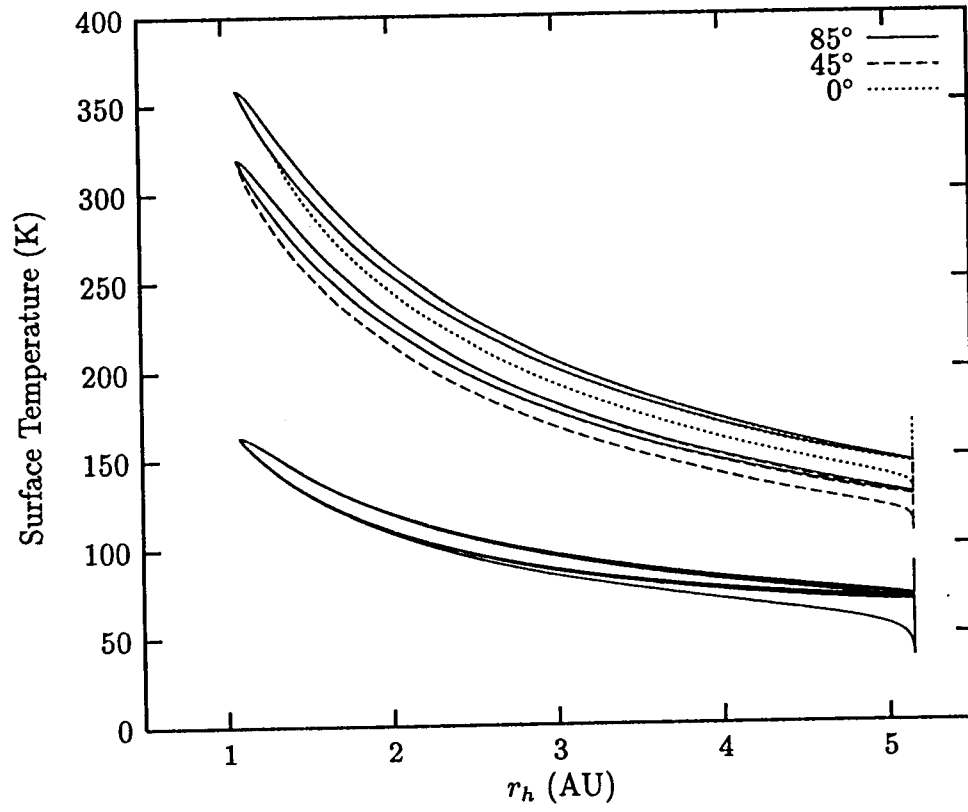


Figure 3: Evolution of the maximum surface temperature versus heliocentric distance for three different latitudes: 85°, 45°, 0°.

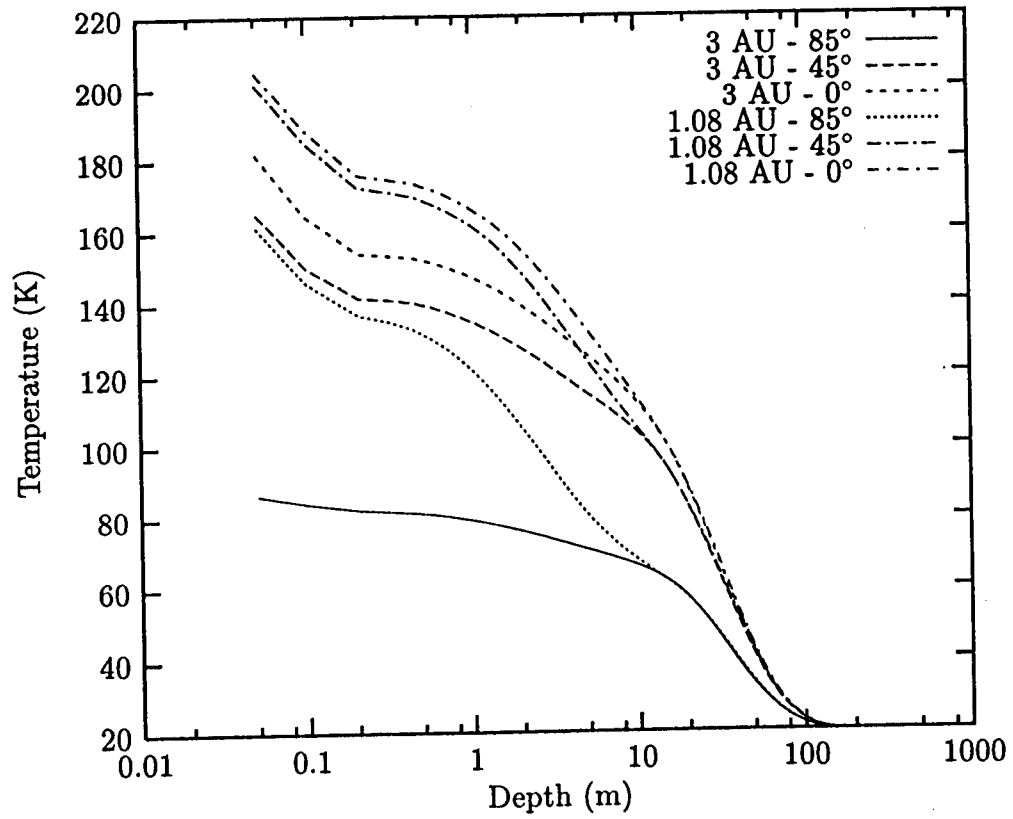


Figure 4: Temperature profiles versus depth after five orbits for 1.08 AU and 3 AU from the Sun and for three different latitudes each at noon, local time.

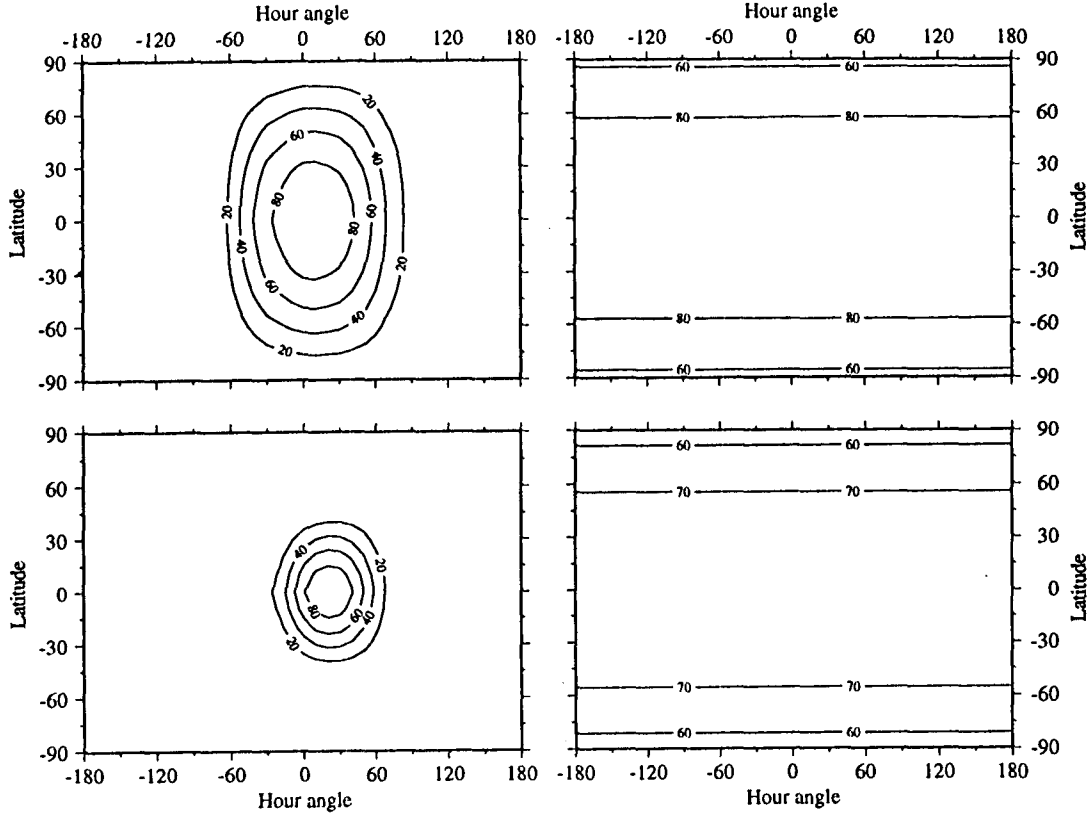


Figure 5: Distribution of gas production at the surface of the modeled comet nucleus with a freely sublimating icy surface at 1.08 AU (top) and 3 AU (bottom) from the Sun, after five orbits. The maximum rate for water production, shown in the two figures at left, is found close to the subsolar point ( $0^\circ$ - $0^\circ$ ) and is set to 100 (units are  $1.11 \times 10^{20}$  molecules  $\text{m}^{-2} \text{s}^{-1}$  for 1.08 AU and  $2.91 \times 10^{18}$  molecules  $\text{m}^{-2} \text{s}^{-1}$  for 3 AU). The offset with respect to the subsolar point is explained by the thermal lag. The distribution of the CO production rate is shown in the two figures at right. The distribution along lines of constant latitude is found to be uniform as the CO source is situated deeper than the diurnal skin depth of a few centimeters. Units are in  $1.61 \times 10^{17}$  molecules  $\text{m}^{-2} \text{s}^{-1}$  for 1.08 AU and  $2.09 \times 10^{17}$  molecules  $\text{m}^{-2} \text{s}^{-1}$  for 3 AU.

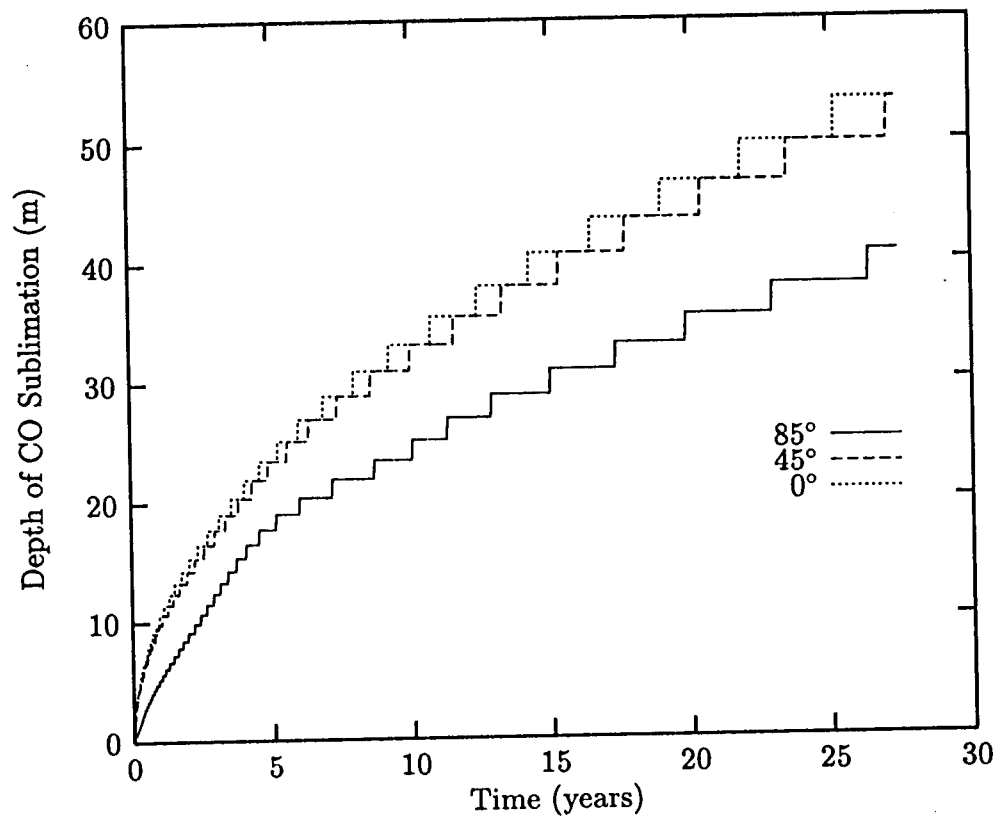


Figure 6: Evolution of the depth of the CO sublimation front versus time for three different latitudes:  $85^{\circ}$ ,  $45^{\circ}$ ,  $0^{\circ}$  .

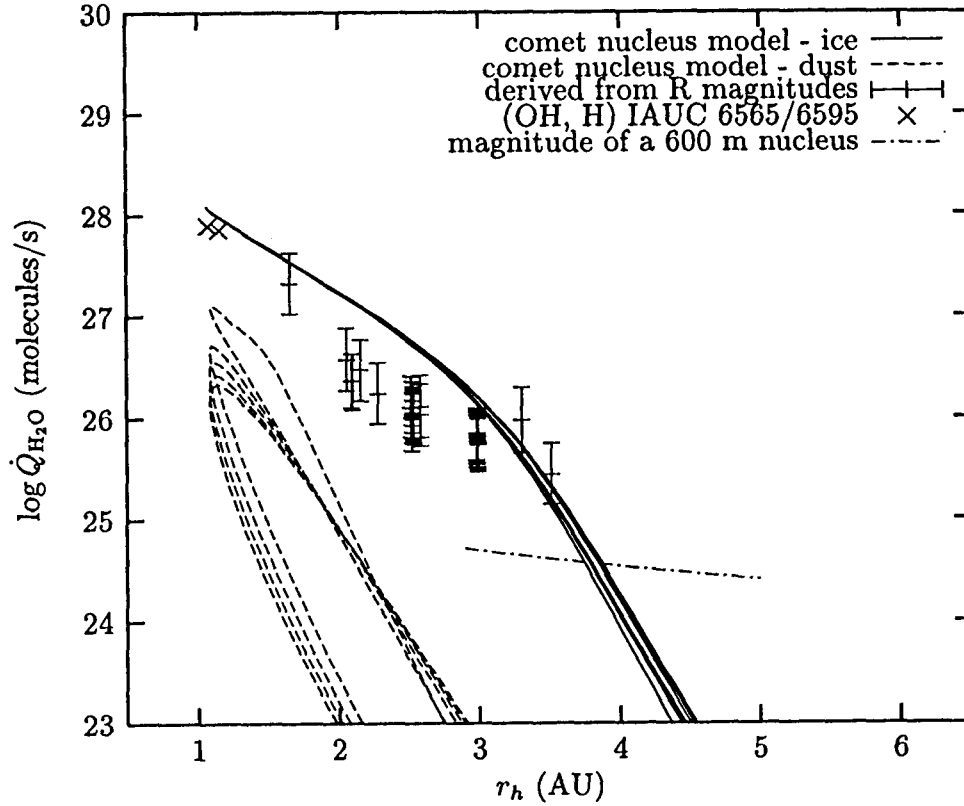


Figure 7: Water production rates versus heliocentric distance. Comparison between the model and observations of comet 46P/Wirtanen in 1995/96. The solid lines correspond to the freely sublimating icy surface, whereas the dashed lines correspond to the dust covered surface and the apparent production rate corresponding to the expected magnitude of a 600 m cometary with an albedo of 0.04. Magnitude data are from a compilation of broadband R magnitudes by Meech *et al.* (1997). Error bars for the measurements of the OH and H production rates were not given in the IAU circulars.

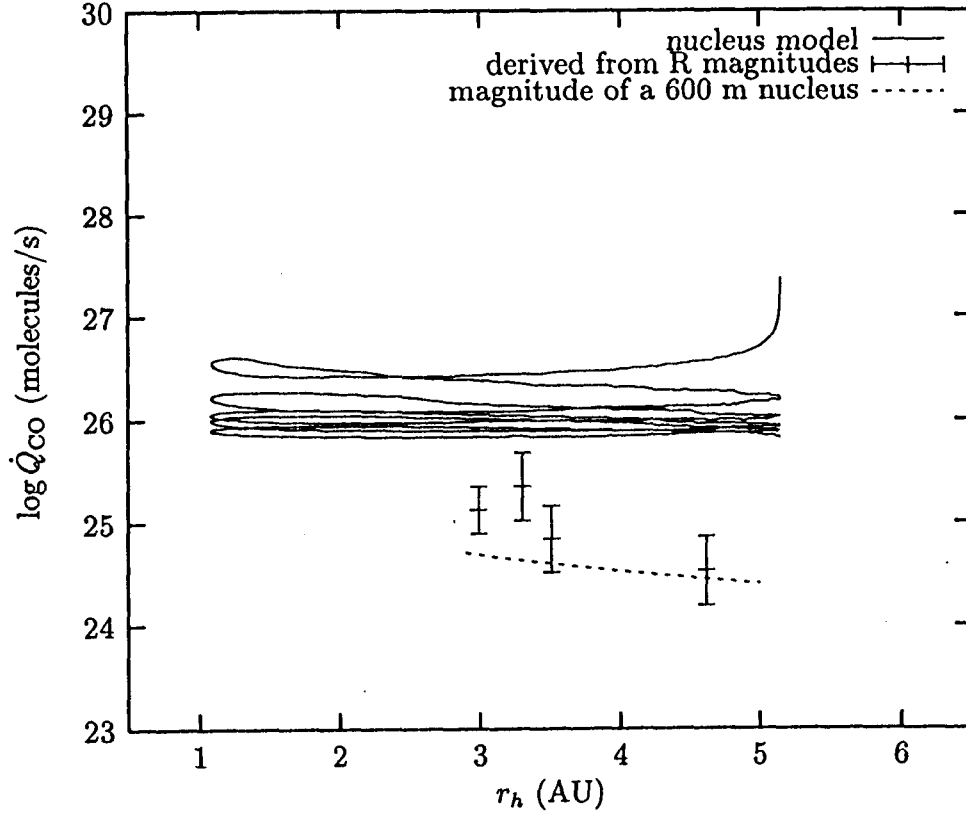


Figure 8: Comparison of modeled carbon monoxide production with production rates derived from the visual brightness of comet 46P/Wirtanen. Magnitude data are from a compilation of broadband R magnitudes by Meech *et al.* (1997). The dashed line shows the apparent production rate corresponding to the expected magnitude of a 600 m cometary nucleus with an albedo of 0.04.